J. Fluid Mech. (2013), *vol.* 737, *pp.* 1–18. © Cambridge University Press 2013
doi:10.1017/jfm.2013.433

Local effects of gravity on foams

Michael J. Davis[1],†, Peter S. Stewart[2] and Stephen H. Davis[1]

[1]Department of Engineering Sciences and Applied Mathematics, McCormick School of Engineering and Applied Science, Northwestern University, Evanston, IL 60208, USA

[2]Oxford Centre for Collaborative Applied Mathematics, Mathematical Institute, The University of Oxford, Oxford OX1 3LB, UK

(Received 22 October 2012; revised 17 May 2013; accepted 13 August 2013; first published online 15 November 2013)

The stability of a two-dimensional surfactant-free (gas–liquid) foam in a gravitational field is considered. The foam is assumed to have low liquid fraction, so the gas phase can be divided into approximately polygonal bubbles separated by thin liquid films. These free films drain toward accumulations of liquid at the bubble vertices, the Plateau borders, and eventually rupture due to van der Waals intermolecular attractions; this drives foam coarsening through the coalescence of neighbouring bubbles. In particular, we demonstrate how gravitational effects strongly modify the shape of the Plateau border interfaces and enhance the drainage flow in the liquid films, driving non-uniform thinning with exponential decay of the minimum film thickness, significantly faster than the power-law thinning predicted when gravitational effects are negligible.

Key words: foams, interfacial flows (free surface), thin films

1. Introduction

A foam is a dispersion of gas bubbles in a liquid phase. When the liquid fraction of a planar foam is sufficiently small, the bubbles are closely packed and take approximately polygonal shapes (Weaire & Hutzler 1999). The bubbles are separated by thin liquid films, called *lamellae*, and the liquid accumulates at the junctions where lamellae meet, known as Plateau borders (PBs). These PBs have highly curved gas–liquid interfaces, resulting in much lower liquid pressures than in the thin lamellae, and therefore exert suction which drives a drainage flow from the films into the borders. When molten metals are foamed with a suitable gas (formed as a precursor to manufacturing porous metal solids), nanoscale particles are added to slow this drainage process (Banhart 2001). However, when the liquid phase is clean, free of surfactants and colloidal particles, the drainage is unopposed and the films thin uniformly (Breward & Howell 2002), where the minimum film thickness decays algebraically in time (Brush & Davis 2005). Once an individual lamella becomes sufficiently thin, van der Waals instabilities can grow to rupture the film in finite time (Anderson, Brush & Davis 2010). On the macroscale, the rupture of an individual lamella can then induce a large-scale topological rearrangement and drive foam coarsening by coalescence of neighbouring bubbles (Stewart & Davis 2012, 2013). However, when the individual foam films are sufficiently long, the extra

† Email address for correspondence: davis@u.northwestern.edu

https://doi.org/10.1017/jfm.2013.433 Published online by Cambridge University Press

liquid flow driven by gravitational forces is non-negligible, significantly modifying the PB drainage and, hence, the stability of the foam; examining how gravity modifies the stability threshold is the focus of the current study.

Gravitational drainage of aqueous foams, where the interfaces are treated with surfactant, has been widely studied. Approaches span between continuum models for the entire foam (Verbist, Weaire & Kraynik 1996; Koehler, Hilgenfeldt & Stone 1999), models of drainage of a single PB (Koehler *et al.* 2002) or models of flow in a single foam lamella (Schwartz & Roy 1999; Naire, Braun & Snow 2000). The latter studies are of most relevance to the present work, where it has been shown that gravitational effects result in exponential thinning of the film for long times (Debrégeas, De Gennes & Brochard-Wyart 1998), compared with power-law thinning for surfactant-free foams where gravity is assumed negligible (Brush & Davis 2005).

The current study looks at the effect of gravity on planar surfactant-free foams, examining the influence on the PB geometry, lamellar drainage and rupture. First, the governing equations are introduced for the liquid phase (§ 2), and then used to construct an outer asymptotic approximation for the PB shape, where the flow is assumed capillary static at leading-order, to examine how the interface shapes are influenced by gravity (§ 3). In § 4, gravitational drainage is studied in a liquid lamella spanning between two vertically aligned PBs, where it is shown that the lamella thins non-uniformly with the minimum thickness decaying exponentially for long time, a solution that is reminiscent of Schultz & Davis (1982) for fibre formation, but with a different geometry and boundary conditions. In addition, using numerical simulations of a reduced model for flow in the lamella (Erneux & Davis 1993), it is shown that non-uniform thinning due to gravity promotes rupture of the film due to van der Waals intermolecular attractions.

2. Governing equations

Consider a planar (two-dimensional) gas–liquid foam in a gravitational field, as depicted in figure 1. When the liquid fraction A_f of the foam is low ($0 < A_f \lesssim 0.1$), the gas bubbles are approximately polygonal, separated by thin liquid films known as *lamellae*; these lamellae intersect in junctions known as PBs, where most of the foam's liquid is located. The liquid phase is assumed to be an incompressible Newtonian fluid with constant viscosity μ and density ρ. The gas phase is assumed to be entirely passive (of negligible density and viscosity compared with the liquid), with each bubble at a uniform pressure. The gas–liquid interface is assumed clean, free of surfactants, with constant surface tension σ. Attraction between the interfaces due to van der Waals forces is captured by a disjoining potential Φ, which we apply as a body force ($=-\nabla\Phi$) to the liquid phase, in a similar matter to Anderson *et al.* (2010). The strength of this potential is proportional to the Hamaker constant for the gas/liquid, denoted as A^*. In addition, the liquid phase experiences an acceleration due to gravity, g.

The liquid lamellae are assumed to be of typical length $2L$ and thickness $2h_0$, and the typical radius of curvature of the gas–liquid interfaces in the PB is assumed to be a_0. We non-dimensionalize by scaling all lengths on L, velocities on $U_0 = (h_0/a_0)^{1/2}(\sigma/\mu)$ (the velocity scale of lamellar drainage; see Brush & Davis 2005), pressures on a capillary scale σ/L, which results in six dimensionless groups

$$\epsilon = \frac{h_0}{L}, \quad \hat{a} = \frac{a_0}{L}, \quad C = \sqrt{\frac{\epsilon}{\hat{a}}}, \quad R = \frac{\rho U_0 L}{\mu}, \quad B = \frac{\rho g L^2}{\sigma}, \quad S = \frac{A^*}{6\pi\sigma L^2}, \qquad (2.1)$$

https://doi.org/10.1017/jfm.2013.433 Published online by Cambridge University Press

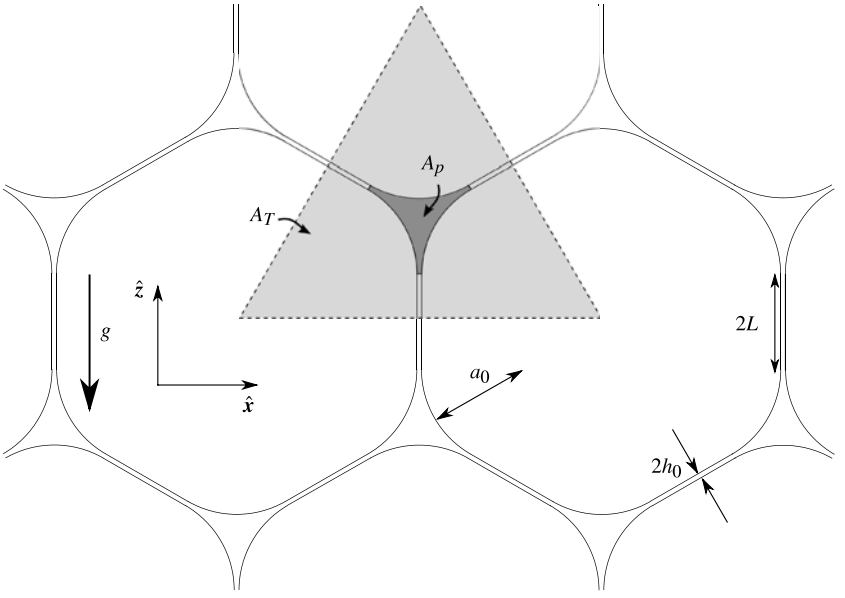


FIGURE 1. Schematic of a planar foam with gravity (dimensional variables).

denoting the the film aspect ratio and the typical PB radius of curvature as well as the capillary, Reynolds, Bond, Sheludko numbers, respectively. In addition, the surrounding gas bubbles are assumed to be of some constant (non-dimensional) pressure, P_j ($j = 1, 2, \ldots$).

The domain is parameterized using a Cartesian coordinate system $\boldsymbol{x} = (x, z)$, where z is aligned opposite to gravity and time is denoted as t. Expressing the liquid velocity field as $\boldsymbol{u}(\boldsymbol{x}, t) = (u, v)$ and pressure as $p(\boldsymbol{x}, t)$, two-dimensional flow in the liquid phase satisfies conservation of mass and momentum, imposed by the Navier–Stokes equations,

$$\boldsymbol{\nabla} \cdot \boldsymbol{u} = 0, \quad CR(\boldsymbol{u}_t + \boldsymbol{u} \cdot \boldsymbol{\nabla}\boldsymbol{u}) = -\boldsymbol{\nabla}(p + \Phi) + C\nabla^2\boldsymbol{u} - B\hat{\boldsymbol{z}}. \tag{2.2a}$$

On the interface with bubble j, denoted as $f_j(\boldsymbol{x}, t) = 0$ ($j = 1, 2, \ldots$), there is continuity of stress, as well as kinematic conditions in the form

$$\hat{\boldsymbol{n}} \cdot \boldsymbol{\Sigma} \cdot \hat{\boldsymbol{n}} = -P_j, \quad \hat{\boldsymbol{t}} \cdot \boldsymbol{\Sigma} \cdot \hat{\boldsymbol{n}} = 0, \quad \frac{\mathrm{d}f_j}{\mathrm{d}t} = 0 \quad \text{on } f_j(\boldsymbol{x}, t) = 0, \ j = 1, 2, \ldots, \tag{2.2b}$$

where $\hat{\boldsymbol{n}}$ and $\hat{\boldsymbol{t}}$ represent unit vectors normal and tangential to the interface, $\boldsymbol{\Sigma}$ represents the liquid stress tensor and $\mathrm{d}/\mathrm{d}t$ refers to the convective derivative.

When the liquid fraction of the foam is low, one can exploit differences in length and velocity scales across the foam to simplify the analysis considerably (Schwartz & Princen 1987; Breward & Howell 2002). For example, assuming that the aspect ratio of the liquid film is small, $\epsilon \ll 1$, allows the governing equations in the lamella to be reduced to one spatial dimension following the procedure outlined by Erneux & Davis (1993). The dimensionless PB curvature $\hat{a}$ is assumed to be $O(1)$ (the semi-arid limit of Brush & Davis 2005), so the corresponding velocity scale ensures that viscous effects are $O(\epsilon^{1/2})$ in the PB. In addition, as shown below, to ensure that van der

https://doi.org/10.1017/jfm.2013.433 Published online by Cambridge University Press

Waals effects balance the pressure gradient along the length of the film, we assume that $S = \epsilon^3 \hat{S}$ with $\hat{S} = O(1)$.

3. Plateau borders

The lowest energy state in planar foams involves hexagonal bubbles and trijunction PBs, so each PB is surrounded by three gas bubbles with (non-dimensional) pressures P_j $(j = 1, 2, 3)$. As in models for dry foams (Weaire & Hutzler 1999), it can be assumed that the amount of liquid in the films is negligible in comparison with the PBs; for a PB in static equilibrium in the absence of gravity, the radius of curvature of each interface is a function of the area of liquid in the PB, A_p, given by

$$A_p = \hat{a}^2 \left(\sqrt{3} - \frac{\pi}{2} \right). \tag{3.1a}$$

The area of the triangular periodic cell surrounding the PB in a hexagonal lattice (A_T, the shaded triangle in figure 1), can then be computed as

$$A_T = \sqrt{3} \left(\sqrt{3} + \hat{a} \right)^2. \tag{3.1b}$$

The area of liquid in a given PB, denoted A_p, can be converted into an approximate foam liquid fraction by comparing to A_T (computed in the absence of gravity), so that $A_f = A_p / A_T$.

For convenience in solving for the shape of the PB, the governing equations can be rescaled using the typical length scale of the PB ($\sqrt{A_p}$), so that

$$\tilde{\boldsymbol{x}} = \sqrt{A_p}\boldsymbol{x}, \quad (\tilde{P}_j, \tilde{p}) = \frac{1}{\sqrt{A_P}}(P_j, p), \quad j = 1, 2, 3. \tag{3.2}$$

Assuming that the Reynolds number of the flow is at most $O(1)$ and $S = O(\epsilon^3)$ (see § 4), at leading order in ϵ the attached lamellae reduce to lines and the rescaled governing equations (2.2) become

$$\tilde{\boldsymbol{\nabla}} \tilde{p} = -B_p \hat{\boldsymbol{z}}, \quad \tilde{P}_j - \tilde{p} = \tilde{\kappa}_j, \quad j = 1, 2, 3, \tag{3.3}$$

where $\tilde{\kappa}_j$ is the (non-constant) curvature of the gas–liquid interface. This outer system is then governed by a single dimensionless group, the modified Bond number $B_p = A_p B$. To leading-order, the total force on the PB is given by

$$\boldsymbol{F} = -\hat{\boldsymbol{z}} \int_{\tilde{A}} B_p \, \mathrm{d}\tilde{\boldsymbol{x}} + \sum_{j=1}^{3} \int_{\tilde{S}_j} \left(\tilde{P}_j - \tilde{p} \right) \boldsymbol{I} \cdot \mathrm{d}\tilde{\boldsymbol{S}}_j; \tag{3.4}$$

this balance is depicted in figure 2.

Solutions to (2.2) are found as a function of B_p. For a PB to be in equilibrium, the net force must be zero ($\boldsymbol{F} = \boldsymbol{0}$). This assumption, coupled with (3.3), yields

$$\boldsymbol{0} = -B_p \hat{\boldsymbol{z}} + \sum_{j=1}^{3} \int_{\tilde{S}_j} \tilde{\kappa}_j \boldsymbol{I} \cdot \mathrm{d}\tilde{\boldsymbol{S}}_j. \tag{3.5}$$

The interface $f_j = 0$ $(j = 1, 2, 3)$ is parameterized using a surface coordinate s_j, where $0 \leqslant s_j \leqslant S_j$, with the orientation chosen to ensure that the unit normal $\hat{\boldsymbol{n}}$ points out of the liquid into the gas. We also use ϕ to denote the angle the tangent to the interface makes with the downwards vertical, and use ϕ_j to denote the angle the lamellar

https://doi.org/10.1017/jfm.2013.433 Published online by Cambridge University Press

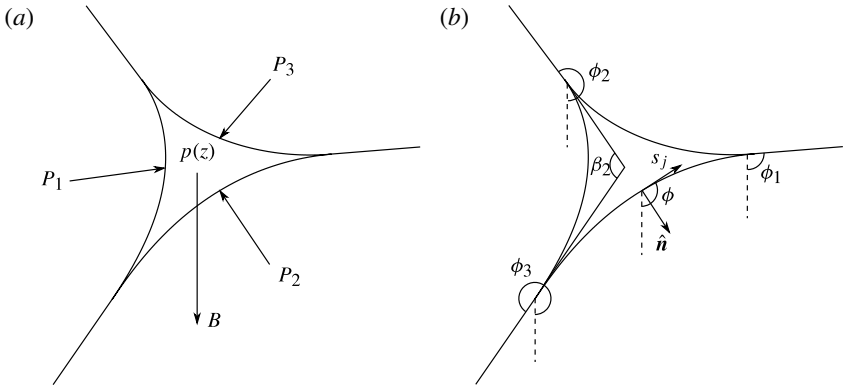


FIGURE 2. Outer asymptotic model for the PB, showing (*a*) the force balance and (*b*) the parameterization of the interface.

midlines make with the downwards vertical, measured counterclockwise, as illustrated in figure 2. It follows that the interface curvature can be expressed as

$$\kappa_j(s_j) = \frac{\partial \phi}{\partial s_j} \quad \text{on } f_j(\boldsymbol{x}, t) = 0, \ \ j = 1, 2, 3, \tag{3.6}$$

where $\mathrm{d}\boldsymbol{S}_j = \hat{\boldsymbol{n}}\,\mathrm{d}s_j$ and $\hat{\boldsymbol{n}} = \cos\phi\hat{\boldsymbol{x}} - \sin\phi\hat{\boldsymbol{z}}$. Balancing forces in the $\hat{\boldsymbol{x}}$ and $\hat{\boldsymbol{z}}$ direction yields

$$\sum_{j=1}^{3} \cos\phi_j = \frac{B_p}{2}, \quad \sum_{j=1}^{3} \sin\phi_j = 0. \tag{3.7}$$

For convenience, the angle swept between adjacent lamellae can be computed as $\beta_j = \phi_{j+1} - \phi_j$, where, for this purpose, $\phi_4 = \phi_1 + 2\pi$.

In order for the asymptotic approximation to be self-consistent, the arcs of the PB must intersect the lamellar midline within a distance of $O(\epsilon^{1/2})$, so that flow induced by this discrepancy does not feature at leading order. Enforcing that the arcs must meet at a single point, along with the constraint that the PBs meet the lamellae tangentially, has the implication that the pressure in the surrounding gas bubbles, P_j, become eigenvalues which must be determined as part of the solution.

3.1. *Numerical results*

Using the constraints that the PBs must meet each other tangentially and at the same point, equation (3.3) can be solved numerically to determine the surrounding gas bubble pressures and the shape of the PBs. First, a starting angle ϕ_1 is chosen, and then by (3.7), the angles ϕ_2 and ϕ_3 are determined. Then, by integrating in s_j along each arc of the PB between these angles (Bashforth & Adams 1883), while imposing the constraint that the arcs form a continuous closed loop, and the scaled area of the border is equal to unity, the shape of the border and the surrounding gas pressures are determined.

In the absence of gravity ($B_p = 0$), the PB shape is governed by surface tension alone, so each gas–liquid interface is a circular arc (constant curvature) that minimizes surface energy (as in Breward & Howell (2002) and Brush & Davis (2005)). In

https://doi.org/10.1017/jfm.2013.433 Published online by Cambridge University Press

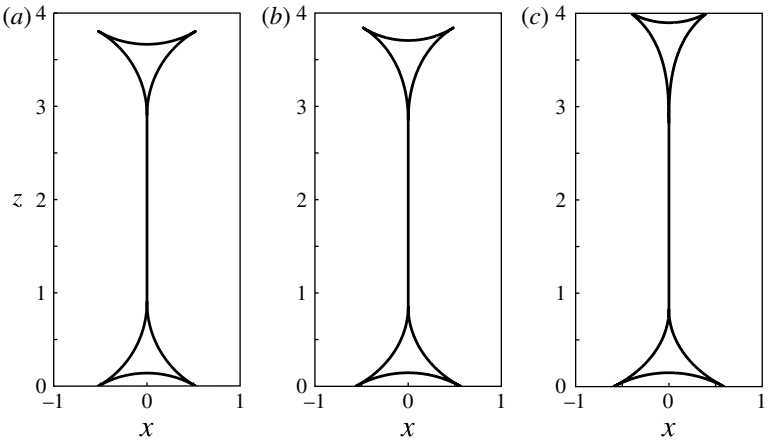


FIGURE 3. Computed PB shapes, plotted in unscaled variables, for various values of Bond number: (*a*) $B = 0$; (*b*) $B = 0.1$; (*c*) $B = 0.175$. The top and bottom PBs are illustrated with a film of length 2 units spanning between them, for foam of an area fraction $A_f = 0.01$. As B increases, the top border becomes thinner and more vertically stretched, while the bottom border becomes wider and vertically compressed.

accordance with Plateau's laws (Plateau 1873), this solution has $\beta_1 = \beta_2 = \beta_3 = 2\pi/3$, independent of PB orientation, which is consistent with (3.7).

With non-zero gravity ($B_p > 0$), the PB shape varies with orientation angle, which influences the sweep angles β_j ($j = 1, 2, 3$), as well as the shapes of the PB arcs. Two particular orientations are considered here, the first where one film is oriented downwards ($\phi_1 = 0$, denoted with subscript t) and the second where one film is oriented upwards ($\phi_2 = \pi$, denoted with subscript b). Typical PB shapes for both orientations, plotted in unscaled variables, are shown in figure 3 for various B_p. Figure 4 illustrates the variation in sweep angle β_j as B_p increases. This demonstrates the asymmetry in the PB shape as a function of ϕ_1 for $B_p > 0$; as B_p increases the top border becomes stretched in the direction of gravity, while the bottom border becomes compressed.

Equation (3.7) gives conditions for the PB to be in quasi-equilibrium, and represents a modification to Plateau's law due to gravity. However, numerical solutions indicate that B_p must not exceed a critical value B_{pc} to ensure the existence of a quasistatic PB, due to the restriction that the PB edges must meet tangentially at the same point. Numerically, it has been determined that $B_{pc} \approx 0.177$. For $B_p > B_{pc}$, there no longer exist quasistatic foam configurations, and PB dynamics must become important at leading order in the foam's evolution. This restriction on B_p suggests that there is a maximum area fraction, A_{fm}, as a function of unscaled Bond number, B, above which quasistatic foams cannot exist. Using (3.1*a*) and (3.1*b*), along with the relations $A_f = A_p/A_T$ and $B_p = A_p B$, makes it possible to express A_{fm} in terms of B and B_{pc} as

$$A_{fm} = \frac{B_{pc}\left(\sqrt{3} - \pi/2\right)}{\sqrt{3}\left(\sqrt{3B\left(\sqrt{3} - \pi/2\right)} + \sqrt{B_{pc}}\right)^2}, \tag{3.8}$$

https://doi.org/10.1017/jfm.2013.433 Published online by Cambridge University Press

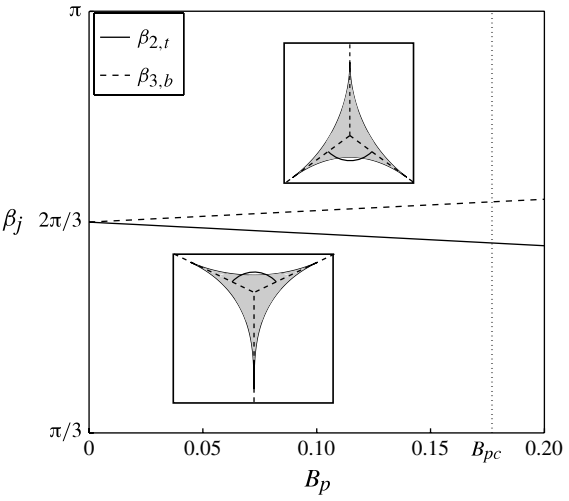


FIGURE 4. PB sweep angles in static equilibrium, as predicted by (3.7), for downwards ($\phi_1 = 0$) and upwards ($\phi_2 = \pi$) oriented PBs. The vertical line shows the maximum value of B_p that allows for static PB shapes; $B_{pc} \approx 0.177$.

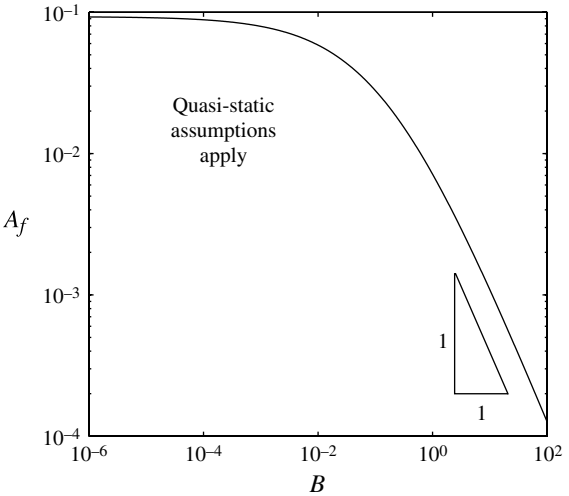


FIGURE 5. Maximum foam liquid fraction, A_{fm}, as a function of Bond number, B. In the limit $B \to \infty$, A_{fm} decays as the inverse of B, so that $A_{fm} \sim B^{-1}$.

which is plotted in figure 5. For area fractions below and to the left of this curve, quasistatic foam configurations exist, and the theory presented in this paper will apply. As $B \to 0$, $A_{fm} \to 1 - \pi/2/\sqrt{3} \approx 0.093$, which is the area fraction at which the jamming transition occurs in planar static foams composed of circular bubbles. As B increases, the maximum permissible area fraction decreases; as the influence of gravity becomes stronger, the amount of liquid that surface tension forces can support becomes smaller.

https://doi.org/10.1017/jfm.2013.433 Published online by Cambridge University Press

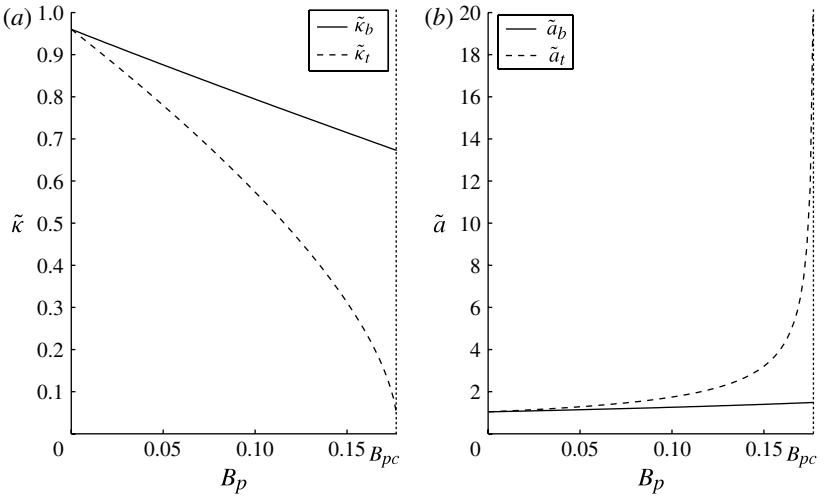


FIGURE 6. Properties of the top (t) and bottom (b) PBs as a function of the PB Bond number B_p: (a) curvature of the gas–liquid interface adjacent to the vertical film; (b) associated radii of curvature of the interfaces.

In § 4 below, a liquid lamella spanning vertically betweens PBs in orientations t and b at the top and bottom of the film, respectively, is considered. In order to match flow in the film to the PB, the radii of curvature of the interface at the point where the PB and film intersect, denoted a_t and a_b for the top and bottom borders respectively, must be determined. The radii are determined by numerically computing the corresponding interfacial curvatures κ_t and κ_b, and using the relation $a_i = 1/\kappa_i$.

In figure 6, numerically determined curvatures, κ_t and κ_b, and associated radii of curvature, a_t and a_b, are shown. As B_p increases, both a_t and a_b increase, as a result of the hydrostatic pressure gradient in the borders driven by gravity. Whereas the increase in a_b is modest the range of allowable B_p, a_t increases much faster because of the additional effect of the vertical pressure gradient due to gravity. Furthermore, a_t diverges as $B_p \to B_{pc}$, at which point the pressure at the bottom of the borders becomes equal to the gas pressure in the surrounding bubbles, and the curvature of the gas–liquid interface goes to zero. Having computed these radii of curvature now allows prediction of drainage flow in the film spanning between the two PBs.

4. A draining film aligned with gravity

Consider a liquid film of dimensionless length 2 units spanning two vertically aligned PBs in orientations t and b (see § 3) at the top and bottom of the film, respectively. Assuming that the aspect ratio of the film is small, $\epsilon \ll 1$, the governing equations can be reduced to one spatial dimension using the methodology outlined by Ida & Miksis (1998). The general form of reduced equations for a free film with arbitrary midline shape is given in equations (46) and (55)–(56) of Ida & Miksis (1998). Their equation is not reproduced here, but a typical geometry is considered where the midline of the film is straight and oriented parallel to the direction of gravity.

The coordinate system is chosen relative to the lamellar midline, where z denotes displacements along the midline from the centre of the film, while x denotes distance

https://doi.org/10.1017/jfm.2013.433 Published online by Cambridge University Press

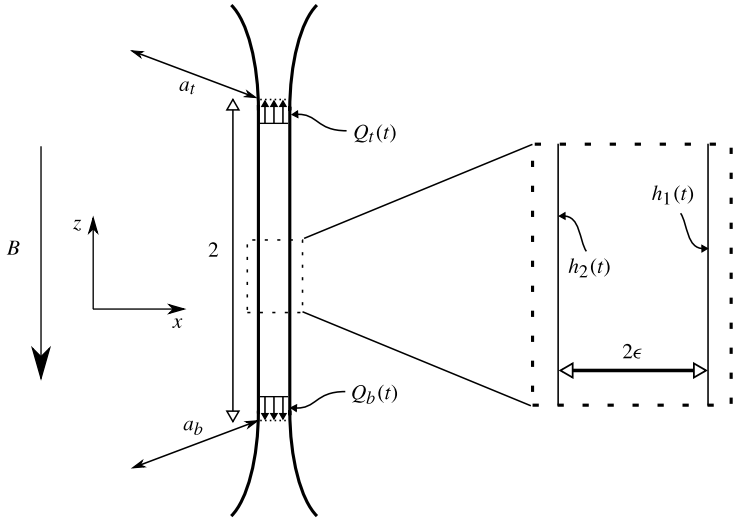


FIGURE 7. Schematic of a vertical lamella with gravity (dimensionless variables).

orthogonal to the midline; the free film interfaces are then denoted as $x = h_1(z, t)$ and $x = h_2(z, t)$, respectively (see dimensionless geometry in figure 7).

In a similar manner to Anderson *et al.* (2010), a disjoining potential proportional to the cube of the normal distance between the interfaces is employed, written in the form (Hamaker 1937; Vrij 1966)

$$\Phi = \frac{S}{(h_1 - h_2)^3}. \tag{4.1}$$

For simplicity, here, it is assumed that the interface profiles are symmetric about $x = 0$, so that $h_1 = -h_2 = h$.

Following Erneux & Davis (1993), a long-wavelength scaling is applied about the lamellar midline, writing the variables in the form

$$t = \hat{t}, \quad (x, z) = (\epsilon\hat{x}, \hat{z}), \quad (u, v) = (\epsilon\hat{u}, \hat{v}), \quad p = \hat{p}, \quad h = \epsilon\hat{h}, \tag{4.2a}$$

and rescale the parameters according to

$$S = \epsilon^3\hat{S}, \quad B = C\hat{B}, \tag{4.2b}$$

where hatted variables and parameters are assumed $O(1)$. The latter choice of rescaling is made to ensure that viscous effects are comparable to gravity along the length of the film. The governing equations (2.2) can then be systematically reduced to the following mass and momentum equations governing lamella evolution ($-1 < \hat{z} < 1$), with error $O(\epsilon^2)$,

$$\hat{h}_{\hat{t}} + \left(\hat{h}\hat{v}\right)_{\hat{z}} = 0, \tag{4.3a}$$

$$\left[RC\left(\hat{v}_{\hat{t}} - \hat{v}\hat{v}_{\hat{z}}\right) - \hat{S}\left(\frac{1}{8\hat{h}^3}\right)_{\hat{z}} - \frac{\epsilon}{2}\hat{h}_{\hat{z}\hat{z}\hat{z}} + C\hat{B}\right]\hat{h} = 4C\left(\hat{h}\hat{v}_{\hat{z}}\right)_{\hat{z}}, \tag{4.3b}$$

where $C = O(\epsilon^{1/2})$.

https://doi.org/10.1017/jfm.2013.433 Published online by Cambridge University Press

To gain insight into the dynamics of lamellar drainage with gravity in the absence of intermolecular attractions ($S = 0$), two approaches are pursued. First, a three region asymptotic decomposition for the foam geometry is constructed, similar to Breward & Howell (2002) (§ 4.1). This approximation is validated by solving the free film equations numerically, using boundary conditions which mimic adjacent PBs (§ 4.2). Then, van der Waals rupture is investigated ($S \neq 0$) using this numerical approach, and the onset of rupture is estimated using a scaling argument (§ 4.3).

4.1. *Three-region asymptotic decomposition*

Solutions of these equations are sought using domain decomposition, a technique first used in Bretherton (1961) (see also Breward & Howell (2002), Brush & Davis (2005)). The inertia of the flow is assumed weak, so that $R = o(1)$, and is not retained at leading-order in any of the asymptotic regions. Also, van der Waals attractions are assumed not to play a role in determining the thinning rate of the film, so for the purpose of predicting drainage it is assumed $S = 0$.

At leading-order, the lamella region ($|\hat{z}| < 1$) is governed by a balance of gravitational and viscous forces and is assumed to be thin, so that the reduced equations (4.3) apply. The PB region ($|\hat{z}| > 1$) is governed by a balance of surface tension and gravity at leading-order (see § 3). The interfaces in these two regions are matched using a narrow transition region, located near $\hat{z} = \pm 1$, described below, where surface tension forces balance viscous forces in the momentum equation, following Breward & Howell (2002).

Since $C = O(\epsilon^{1/2})$, the leading-order equations in the lamella region are given by

$$\hat{h}_{\hat{t}} + \left(\hat{h}\hat{v}\right)_{\hat{z}} = 0, \quad \hat{B}\hat{h} = \left(\hat{h}\hat{v}_{\hat{z}}\right)_{\hat{z}}, \quad (-1 < \hat{z} < 1). \tag{4.4a}$$

Denoting the liquid fluxes into the PBs from the top and bottom of the lamellar region as Q_t and Q_b, respectively, it is possible to impose velocity boundary conditions in the edges of the lamellar region in the form

$$\hat{v}(-1, \hat{t}) = -\frac{Q_t(\hat{t})}{\hat{h}(-1, \hat{t})}, \quad \hat{v}(1, \hat{t}) = \frac{Q_b(\hat{t})}{h(1, \hat{t})}. \tag{4.4b}$$

Matching between the PB and the lamellar regions requires consideration of transition regions of width δ_t and δ_b at the ends of the film; these are assumed to be narrow to allow viscous forces to balance surface tension forces at leading-order. The matching follows closely to what is done in Breward & Howell (2002), but allowing for a non-uniform profile across the lamellar region and a non-constant PB curvature (due to gravity). Having viscous and surface tension effects balance in the transition region, along with the assumption that the PB interface radius of curvature is $O(1/\hat{a})$, leads to the scalings

$$\delta_b = \delta_t = \sqrt{\epsilon \hat{a}}. \tag{4.5a}$$

In a similar manner to Breward & Howell (2002), the flux of liquid is spatially uniform across the transition region; we can then integrate the transition region equations exactly to compute the flux draining into the PB at each end,

$$Q_b = \frac{3(2\hat{a})^{1/2}\hat{h}(-1, \hat{t})^{3/2}}{16 a_b{}^{1/2}}, \quad Q_t = \frac{3(2\hat{a})^{1/2}\hat{h}(1, \hat{t})^{3/2}}{16 a_t^{1/2}}, \tag{4.5b}$$

https://doi.org/10.1017/jfm.2013.433 Published online by Cambridge University Press

where a_b and a_t are the radii of curvature at the edge of the top and bottom PBs, as defined in § 3.

The general solution of (4.4*a*) for $\hat{t} > 0$ is given by

$$\hat{h}(\hat{z},\hat{t}) = f_1(\hat{t})\mathrm{e}^{-\hat{B}\hat{z}\hat{t}}, \quad \hat{v}(\hat{z},\hat{t}) = f_2(\hat{t}) + f_3(\hat{t})\mathrm{e}^{\hat{B}\hat{z}\hat{t}} - \hat{z}/\hat{t}. \tag{4.6}$$

Using the boundary conditions (4.4*b*) with the fluxes Q_b and Q_t given in (4.5*b*) allows for analytic solutions for $f_2(t)$ and $f_3(t)$ in the form

$$f_2(\hat{t}) = -\frac{\coth(\hat{B}\hat{t})}{t} - \frac{(Q_b + Q_t)\,\mathrm{csch}(\hat{B}\hat{t})}{2f_1(\hat{t})}, \tag{4.7a}$$

$$f_3(\hat{t}) = \frac{(\coth(\hat{B}\hat{t}) - 1)\left[\left(\mathrm{e}^{2\hat{B}\hat{t}}Q_b + Q_t\right)\hat{t} + 2\mathrm{e}^{\hat{B}\hat{t}}f_1(\hat{t})\right]}{2\hat{t}f_1(\hat{t})}, \tag{4.7b}$$

where the fluxes can be written as

$$Q_b = \frac{3(2\hat{a})^{1/2}f_1(\hat{t})^{3/2}\mathrm{e}^{3\hat{B}\hat{t}/2}}{16{a_b}^{1/2}}, \quad Q_t = \frac{3(2\hat{a})^{1/2}f_1(\hat{t})^{3/2}\mathrm{e}^{-3\hat{B}\hat{t}/2}}{16{a_t}^{1/2}}. \tag{4.7c}$$

Substituting the forms of $\hat{h}(\hat{z},\hat{t})$ and $\hat{v}(\hat{z},\hat{t})$ given in (4.6) into (4.4*a*) results in an ODE for the evolution of $f_1(\hat{t})$, given by

$$f_1'(\hat{t}) - f_1(\hat{t})\left(\hat{B}\hat{t}f_2(\hat{t}) + 1/\hat{t}\right) = 0, \quad (\hat{t} > 0) \tag{4.8}$$

where $f_2(\hat{t})$ is given in (4.7*a*). Hence, (4.8) is a nonlinear, first-order ODE for $f_1(\hat{t})$, which can easily be integrated numerically to predict the thinning rate of the film. In the limit of weak gravity ($\hat{B} \ll 1$), it can be shown that at leading-order, the solution reduces to the results of Breward & Howell (2002), giving a second-order power-law thickness decay. In the limit of strong gravity, $\hat{B} \to 0$, it can be shown that at leading-order, $f_1(\hat{t}) \sim \hat{B}\hat{t}\,\mathrm{csch}\left(\hat{B}\hat{t}\right)$. It can also be shown that for long times, $\hat{h}(1,\hat{t})$ decays exponentially for all $\hat{B} \neq 0$.

Equation (4.8) is solved numerically by starting at a time just greater than zero ($\hat{t} = 0^+$), and integrating forward. Computing these solutions for $\hat{B} = 0$ and $\hat{B} = 5$, the thickness at the ends of the lamellar region, as well as the corresponding drainage fluxes into the PB, are shown in figure 8. In the absence of gravity, the drainage is symmetric (Breward & Howell 2002). However, with gravity, the film profile quickly becomes bulged at the bottom end and constricted at the top (figure 8*a*) and the drainage rate is modified both by the change in curvatures of the PB and by the non-uniform thinning of the film (figure 8*b*). Initially, when the film is flat, the drainage rate into the bottom border is slightly greater ($Q_b > Q_t$) due to differences in curvature at the ends of the film (figure 6*b*), but this difference is quite small. However, the film rapidly adopts a non-uniform profile (figure 8*a*) due to gravitational flow within the lamella, which drives a huge difference in the drainage rates between the top and bottom of the lamella (figure 8*b*).

4.2. *Numerical results*

The domain decomposition predictions of § 4.1 are verified by comparison with numerical solutions of the full PDE system (4.9) across a domain which encompasses

https://doi.org/10.1017/jfm.2013.433 Published online by Cambridge University Press

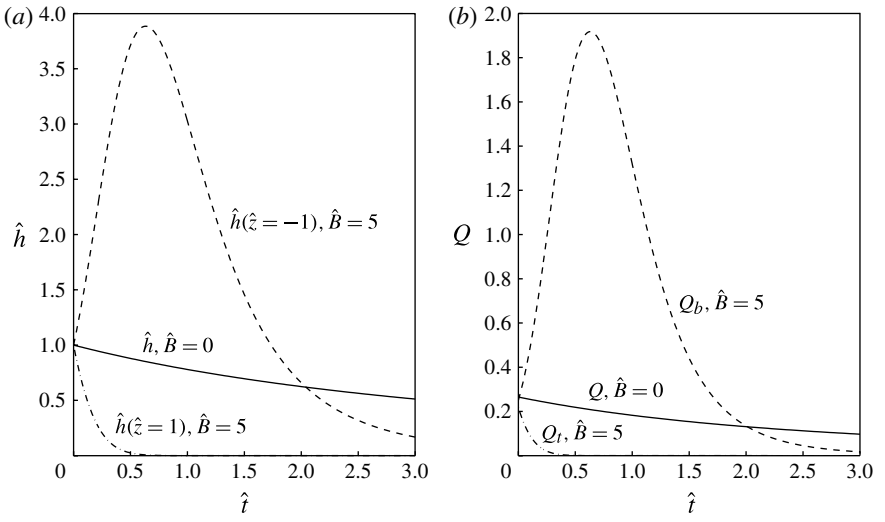


FIGURE 8. Asymptotic model of vertical film draining under gravity for $\hat{B}=5$: (*a*) film thickness at the top (dot-dashed line) and bottom (dashed line) of the lamellar region; (*b*) the corresponding drainage flux oriented into the adjacent PB. In both subplots the solid line corresponds to a uniformly thinning foam lamella in the absence of gravity. Here, the area fraction of the PBs is $A_f = 0.01$.

both the lamella and a small portion of the surrounding PBs, denoted as $-\mathscr{L} < z < \mathscr{L}$, where $\mathscr{L} > 1$. Undoing the asymptotic scaling (4.2) to return to $O(1)$ variables, the reduced governing equations across the film (4.3) ($-\mathscr{L} < z < \mathscr{L}$) become

$$h_t + (hv)_z = 0, \tag{4.9a}$$

$$\left[RC\,(v_t + vv_z) - S\left(\frac{1}{8h^3}\right)_z - \frac{1}{2}\left(\frac{h_{zz}}{(1+h_z^2)^{3/2}}\right)_z + B\right] h = 4C(hv_z)_z; \tag{4.9b}$$

subject to

$$h_{zz}(z=-\mathscr{L}) = 1/a_b, \quad h_{zz}(z=\mathscr{L}) = 1/a_t, \tag{4.9c}$$

where $h(z,0) = O(\epsilon)$. Note that in these equations the full expression for the free surface curvature has been retained, since this improves the approximation in the PBs, and that the gravity term features in the momentum equations, which is not considered in Ida & Miksis (1998).

To solve the PDE (4.9), second-order spatial finite-differences are used with semi-implicit (first-order) time stepping, treating only the highest derivative in each equation implicitly. A constant curvature is imposed at each edge of the PB, valid under the assumption that the PBs do not swell significantly due to drainage flow (consistent with the semi-arid limit of Brush & Davis (2005)). These curvatures are chosen consistently with predictions from § 3, shown in figure 6, consistent with a liquid area fraction of $A_f = 0.01$. This area fraction has quasistatic PB solutions for all values of B used in this section (see figure 5). To close the system, no flow at the edges of the domain is assumed (i.e. flow is negligible in the adjoining PBs), consistent with the outer asymptotic approximation in § 3. These assumptions are expected to be suitable when the initial lamella thickness is sufficiently small.

https://doi.org/10.1017/jfm.2013.433 Published online by Cambridge University Press

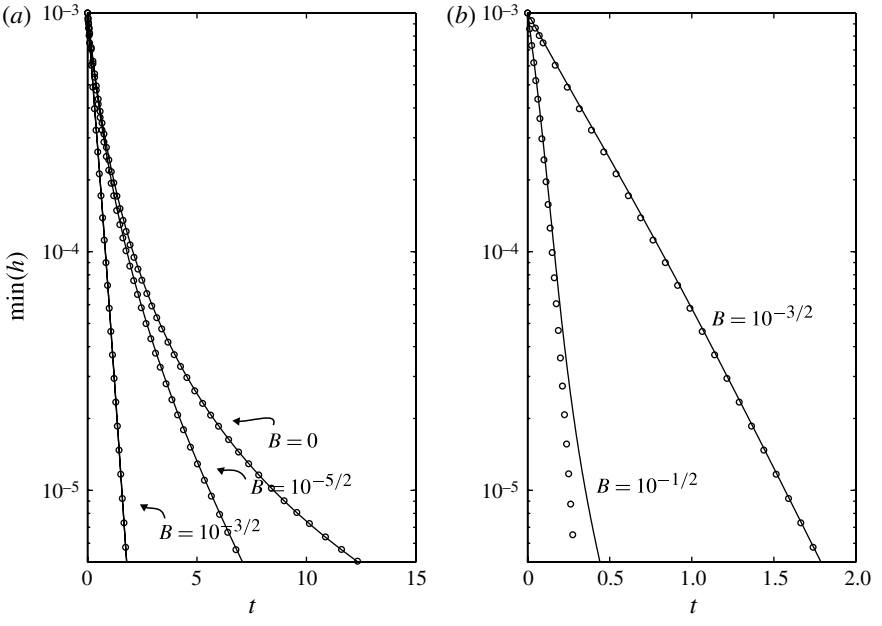


FIGURE 9. Comparison of numerically computed thinning rates (solid lines) with the asymptotic predictions (open circles) for vertical draining between PBs with area fraction $A_f = 0.01$ and film aspect ratio $\epsilon = 10^{-3}$: (*a*) minimum film thickness for relatively small B; (*b*) minimum film thickness for larger B.

Figure 9 shows a comparison of the minimum film thickness (which occurs near $z = 1$) as predicted using domain decomposition with those computed numerically; the predictions match the computations very well for values of B up to 1, but the asymptotic predictions deviate somewhat for larger values of Bond number at long times. However, even for small B, one can see that gravity greatly enhances the thinning rate, and that for long times the minimum film thickness decays exponentially, in contrast to the power-law thinning law predicted for lamellae without gravity (Brush & Davis 2005). The numerical simulations also indicate that solving (4.6)–(4.8) provides accurate predictions of thinning rates for $B \lesssim 10^{-1/2} \approx 0.32$, with much reduced computational cost.

Figure 10 shows a comparison between the lamella shape as predicted by (4.6)–(4.8) with the shape computed from the full numerical solutions of (4.9). As expected, for $B = 10^{-5/2} \approx 3.2 \times 10^{-3}$, there is excellent agreement between the two (figure 10*a*,*c*), but deviations occur for $B = 0.1$, which is clear from the velocity profiles (figure 10*d*): the asymptotic model over-predicts the thinning rate of the film in this case, since it neglects surface tension forces in the lamellar region. As the free surface becomes increasingly curved, the curvature gradient h_{zzz} becomes large, and the surface tension term in (4.9*b*) is no longer negligible. These surface tension forces slow the thinning due to gravity, which explains why the reduced model over-predicts thinning rates for large B.

4.3. *van der Waals rupture*

In the absence of a disjoining pressure ($S = 0$), the film will never rupture in finite time; film rupture requires disjoining pressure (Vrij 1966). In figure 11(*a–d*), the

https://doi.org/10.1017/jfm.2013.433 Published online by Cambridge University Press

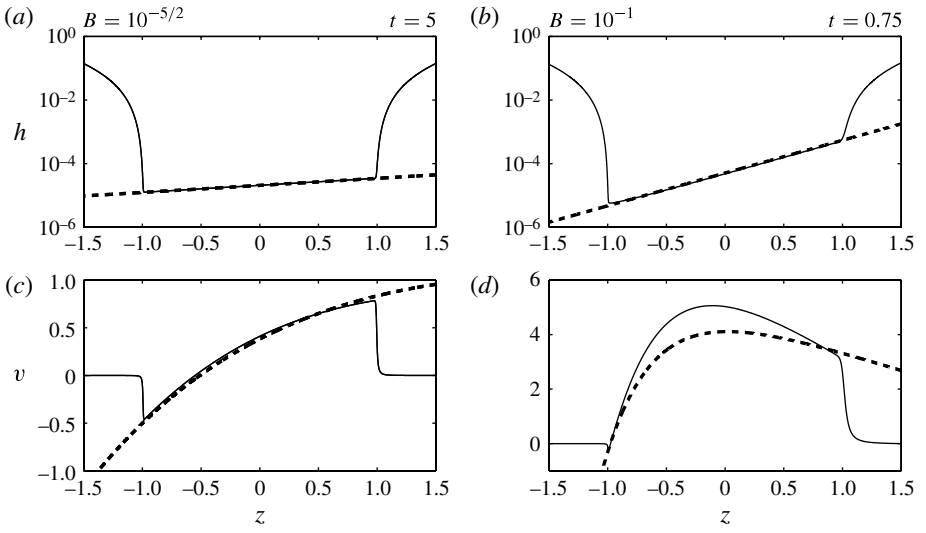


FIGURE 10. Numerically computed flow profiles for $\epsilon = 10^{-3}$ and $A_f = 0.01$ (solid lines) compared to asymptotic predictions (dashed lines): (*a*) film thickness for $B = 10^{-5/2}$ at time $t = 5$ units; (*b*) film thickness for $B = 10^{-1}$ at time $t = 0.75$; (*c*) streamwise flow velocity for $B = 10^{-5/2}$ at time $t = 5$; (*d*) streamwise flow velocity for $B = 10^{-1}$ at time $t = 0.75$.

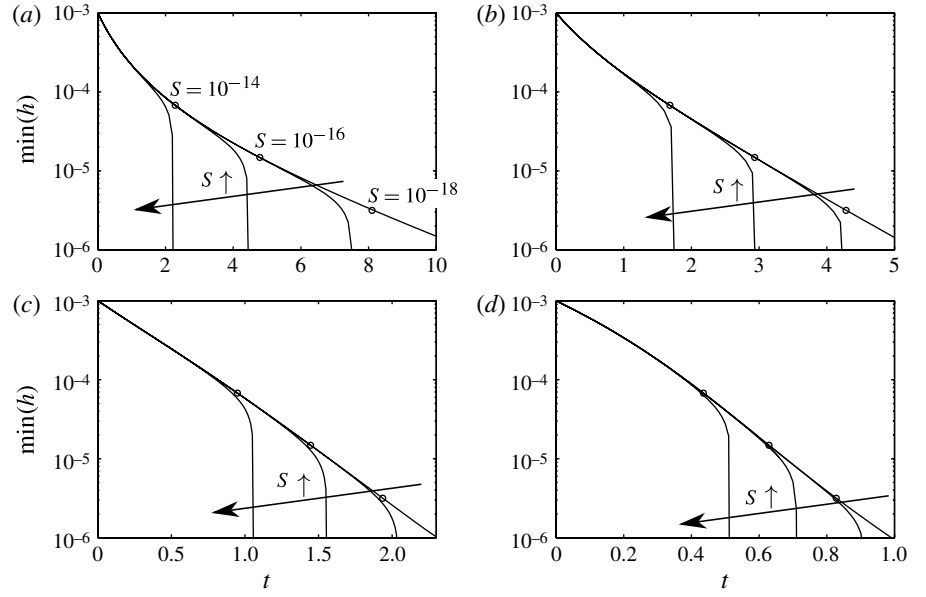


FIGURE 11. Minimum thickness of the foam lamella for $\epsilon = 10^{-3}$ and $A_f = 0.01$ for $S = 10^{-14}, 10^{-16}, 10^{-18}$: (*a*) $B = 10^{-2}$; (*b*) $B = 10^{-3/2}$; (*c*) $B = 10^{-1}$; (*d*) $B = 10^{-1/2}$. Also shown in each part is the corresponding curve for $S = 0$, for which the film does not rupture in finite time. The open circles indicate rupture points as predicted by scaling arguments (4.10).

https://doi.org/10.1017/jfm.2013.433 Published online by Cambridge University Press

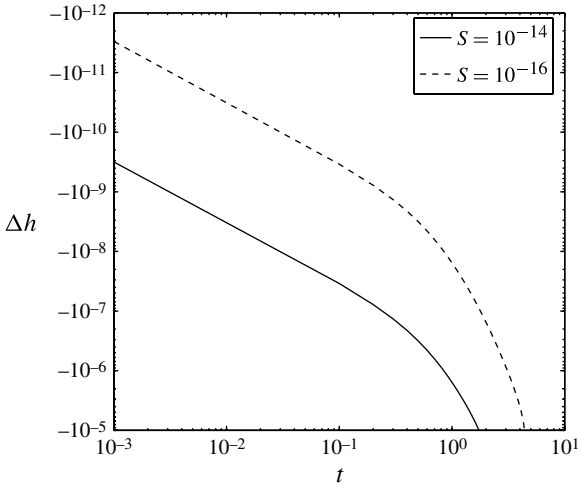


FIGURE 12. Difference in the film thickness at the top end of the lamella $h(1, t)$ between curves computed for $S = 0$ and $S \neq 0$ ($S = 10^{-14}, 10^{-16}$), with $\epsilon = 10^{-3}$, $A_f = 0.01$ and $B = 10^{-2}$.

evolution of the minimum film thickness is compared for various S and B. While the film thins indefinitely without rupture for $S = 0$, the film will rupture in finite time for all $S \neq 0$, and the computed time until rupture decreases as the Sheludko number increases, when starting from identical initial conditions.

Anderson *et al.* (2010) considered the stability of drainage flow in a flat foam lamella in the absence of gravity, showing that the film becomes unstable at some critical thickness. However, the onset of instability is not so clear in the present case where the non-uniform film profile is continuously modified by the disjoining pressure; for example, figure 12 shows the difference between the lamellar thickness for $S = 0$ and $S \neq 0$ at $z = 1$, denoted $\Delta h(t)$, when starting at identical initial conditions. There is a marked separation between the curves for $S = 0$ and $S \neq 0$ (see figure 12); this separation grows as the film becomes thinner, until eventually there is a sharp deviation toward film rupture. At a critical thickness the film profile transitions from being stable to unstable; this instability then grows toward rupture in finite time. However, the basic draining state is modified by intermolecular attractions, so there is no longer a clear distinction between the thinning and rupture phases of lamellar evolution.

It is expected that the onset of rupture occurs once the disjoining pressure grows to be large enough to balance the viscous dissipation term in the momentum equation (4.3*b*). For an $O(1)$ flow velocity, this suggests that the film will rupture when the minimum thickness approaches a critical value

$$h_c \sim \left(\frac{S}{4C}\right)^{1/3} = \left(\frac{A^* a_0^{1/2}}{24\pi\gamma L^2 h_0^{1/2}}\right)^{1/3}. \tag{4.10}$$

This prediction is plotted against each simulation run in figure 11, observing good agreement with the onset of rupture in the numerical simulations. For all cases tested, the rupture time is within 10 % of the predicted time. It should be noted that (4.10) implies that $S \sim h_c^3$, which is consistent with past results for critical film thickness in

https://doi.org/10.1017/jfm.2013.433 Published online by Cambridge University Press

Liquid phase	ρ (kg m^{-3})	σ (N m^{-1})	L (m)	B
Aluminum	2.4×10^3	1.0×1	10^{-2}	2.4
			10^{-4}	2.4×10^{-4}
Water	1.0×10^3	7.3×10^{-2}	10^{-2}	1.4×10^{1}
			10^{-4}	1.4×10^{-1}

TABLE 1. Typical values of Bond number, B, for foams composed of molten aluminum and water, for films of various lengths.

the presence of drainage and PBs (Anderson *et al.* 2010). Equation (4.10) also implies that while gravity strongly influences the thinning rate of the lamella, it does not feature in determining the critical thickness for the onset of instability.

5. Discussion

Using a combination of asymptotic analysis and numerical simulation, the present work examined the role of gravity in the breakdown of planar foams. In particular, the gas and liquid phases phases have been assumed clean, free of surfactants and colloidal particles, relevant to batch-processing methods for the production of molten metallic foams as a precursor to forming porous metal solid (Banhart 2001).

The foam has been assumed to be entirely two-dimensional, so drainage flows are oriented only along the liquid films toward the PBs. However, in three-dimensional foams there can also be significant gravitational drainage along the PBs themselves, which require alternative approaches (Weaire & Hutzler 1999; Koehler *et al.* 2002).

The model employed an outer asymptotic approximation for liquid flow in the PB, where at leading order the adjoining liquid films map to lines and the gas–liquid interfaces meet tangentially (and at a point). Velocities were scaled using the typical drainage flow speed in the liquid film (Breward & Howell 2002; Brush & Davis 2005), with the added consequence that the the PB flow can be considered as capillary static at leading order. Numerical computations of the PB interface shapes showed that Plateau's laws are modified by gravity, in that the angles swept out between adjacent lamellae when the PB is in static equilibrium are no longer equal (figure 4). In addition, there is a maximal liquid fraction for the existence of capillary static PBs (figure 5). This threshold is equally applicable to studies in static aqueous foams in a gravitational field (Weaire & Hutzler 1999). In the absence of gravity, this threshold liquid fraction corresponds to the jamming transition for circular bubbles in a planar foam. However, this threshold liquid fraction decreases significantly as the Bond number of the system increases, indicating that gravitational effects inhibit the stability of the PB. For example, in molten aluminum foams with films of typical length 1 cm, the maximal admissible liquid fraction for a static PB is approximately 1 % (an estimate of the Bond number is given in table 1). Full PB computations (using the boundary-integral method or similar) would then be necessary to understand their behaviour for larger liquid fractions, but it is conceivable that their dynamics would contribute to foam breakdown.

The drainage and rupture of the liquid films joining these PBs has also been considered, using a combination of domain decomposition (following Breward & Howell 2002) and numerical simulation. Attention was restricted to a film with midline oriented vertically (to allow symmetry arguments to be exploited), but the analysis can be readily extended to films with arbitrary orientation or curvature. Gravitational

https://doi.org/10.1017/jfm.2013.433 Published online by Cambridge University Press

effects result in a much faster rate of lamellar drainage toward the lower PB (figure 8) through a combination of two mechanisms: first, the pressure drop between the film and the lamella, which drives capillary-viscous suction, is less at the upstream end of the film because of curvature difference in the PBs (figure 6); secondly, and much more significantly, gravitational effects result in a highly non-uniform film profile, where the film is bulged at the lower end and constricted at the upper end (figure 10), which allows larger amounts of liquid to move into the lower PB. The minimum film thickness decays exponentially for long times, in accordance with studies of gravitational drainage in aqueous foams (for example Schwartz & Roy 1999), as opposed to power-law thinning observed in the absence of gravity (Brush & Davis 2005). Intermolecular attractions can then grow to rupture the film in finite time. However, a scaling argument suggested that the onset of instability is dependent only on the minimum film thickness, approximately independent of gravity, and governed by a balance between disjoining pressure and viscous forces (as in Anderson *et al.* (2010)).

Having constructed reduced models for the PB and film regions, it could prove illuminating to couple these into a larger scale representation of the foam (perhaps using a network modelling approach similar to Stewart & Davis 2012, 2013) to consider macroscopic rheology in a gravitational field, but this is deferred to future work.

Acknowledgements

The authors gratefully acknowledge funding from the NSF grant CMMI-0826703. Michael would also like to acknowledge additional funding from the NSF RTG grant DMS-0636574, and from a Cabell fellowship provided by the McCormick School of Engineering and Applied Science at Northwestern University.

REFERENCES

ANDERSON, A. M., BRUSH, L. N. & DAVIS, S. H. 2010 Foam mechanics: spontaneous rupture of thinning liquid films with Plateau borders. *J. Fluid Mech.* **658**, 63–88.

BANHART, J. 2001 Manufacture, characterisation and application of cellular metals and metal foams. *Prog. Mater. Sci.* **46** (6), 559–632.

BASHFORTH, F. & ADAMS, J. C. 1883 *An Attempt to Test the Theories of Capillary Action: By Comparing the Theoretical and Measured Forms of Drops of Fluid*. Cambridge University Press.

BRETHERTON, F. P. 1961 The motion of long bubbles in tubes. *J. Fluid Mech.* **10**, 166–188.

BREWARD, C. J. W. & HOWELL, P. D. 2002 The drainage of a foam lamella. *J. Fluid Mech.* **458**, 379–406.

BRUSH, L. N. & DAVIS, S. H. 2005 A new law of thinning in foam dynamics. *J. Fluid Mech.* **534**, 227–236.

DEBRÉGEAS, G., DE GENNES, P. G. & BROCHARD-WYART, F. 1998 The life and death of 'bare' viscous bubbles. *Science* **279**, 1704–1707.

ERNEUX, T. & DAVIS, S. H. 1993 Nonlinear rupture of free films. *Phys. Fluids* A-*Fluid* **5**, 1117.

HAMAKER, H. C. 1937 The Londonvan der Waals attraction between spherical particles. *Physica* **4**, 1058–1072.

IDA, M. P. & MIKSIS, M. J. 1998 The dynamics of thin films I: general theory. *SIAM J. Appl. Maths* 456–473.

KOEHLER, S. A., HILGENFELDT, S. & STONE, H. A. 1999 Liquid flow through aqueous foams: the node-dominated foam drainage equation. *Phys. Rev. Lett.* **82**, 4232–4235.

KOEHLER, S. A., HILGENFELDT, S., WEEKS, E. R. & STONE, H. A. 2002 Drainage of single Plateau borders: direct observation of rigid and mobile interfaces. *Phys. Rev.* E **66**, 040601.

https://doi.org/10.1017/jfm.2013.433 Published online by Cambridge University Press

MYSELS, K. J., FRANKEL, S. & SHINODA, K. 1959 *Soap Films: Studies of Their Thinning and a Bibliography,* vol. 230, pp. 91–106. Pergamon.

NAIRE, S., BRAUN, R. J. & SNOW, S. A. 2000 An insoluble surfactant model for a vertical draining free film. *J. Colloid Interface Sci.* **230**, 91–106.

PIGEONNEAU, F. & SELLIER, A. 2011 Low-Reynolds-number gravity-driven migration and deformation of bubbles near a free surface. *Phys. Fluids* **23**, 92–102.

PLATEAU, J. A. F. 1873 *Statique expérimentale et théorique des liquides soumis aux seules forces moléculaires*. Gauthier Villars.

SCHULTZ, W. W. & DAVIS, S. H. 1982 One-dimensional liquid fibres. *J. Rheol.* **26**, 331–345.

SCHWARTZ, L. W. & PRINCEN, H. M. 1987 A theory of extensional viscosity for flowing foams and concentrated emulsions. *J. Colloid Interface Sci.* **118**, 201–211.

SCHWARTZ, L. W. & ROY, R. V. 1999 Modelling draining flow in mobile and immobile soap films. *J. Colloid Interface Sci.* **218**, 309–323.

STEWART, P. S. & DAVIS, S. H. 2012 Dynamics and stability of metallic foams: network modelling. *J. Rheol.* **56** (3), 543–574.

STEWART, P. S. & DAVIS, S. H. 2013 Self-similar coalescence of clean foams. *J. Fluid Mech.* **722** (3), 645–664.

VERBIST, G., WEAIRE, D. & KRAYNIK, A. M. 1996 The foam drainage equation. *J. Phys.: Condens. Matter* **8**, 3715–3731.

VRIJ, A. 1966 Possible mechanism for the spontaneous rupture of thin, free liquid films. *Discuss. Faraday Soc.* **42**, 23–33.

WEAIRE, D. & HUTZLER, S. 1999 *The Physics of Foams*. Oxford University Press.

https://doi.org/10.1017/jfm.2013.433 Published online by Cambridge University Press